Iranian (Iranica) Journal of Energy & Environment
Journal Homepage: www.ijee.net
IJEE an official peer review journal of Babol Noshirvani University of Technology, ISSN:2079-2115

Performance Augmentation of Solar Air Heater for Space Heating Using a Flexible Flapping Guide Winglet

S. A. Gandjalikhan Nassab*, M. Moein Addini

Department of Mechanical Engineering, School of Engineering, Shahid Bahonar University of Kerman, Kerman, Iran

P A P E R I N F O

Paper history:
Received 16 February 2021
Accepted in revised form 09 April 2021

Keywords:
Heat transfer enhancement
Solar air heaters
Space heating
Vortex generator

A B S T R A C T

A new idea is presented in this paper for improving the performance of solar air heater (SAH) designed for space heating by employing a thin flexible guide winglet. In addition to the role of winglet in pushing the convective airflow toward the heated surface, it behaves as a vortex generator (VG) due to its vibration by fluid-solid interaction (FSI) that causes flow mixing and breaking thermal boundary layer. In flow simulation, the finite element method (FEM) is employed with considering a two-way strongly-coupled FSI approach at transient condition. Numerical solution of the governing equations, including the continuity, momentum and energy for convective flow and the equation of motion for VG are obtained by COMSOL multi-physics. The well-known $k-\varepsilon$ model is employed for computation of turbulent stress and heat flux. The present numerical results are validated against the most recent relevant literature. To provide a clear and deep understanding of the proposed concept, extensive comparisons are made between different test cases. Results reveal considerable performance enhancement of SAH with elastic guide winglet compared with clean solar air heater (CSAH), such that 56% increase in the natural airflow rate and 9% decrease in the average absorber temperature is seen because of the flapping winglet. But, the air outlet temperature decreases about 14% due to flapping VG. This study aims to make the proposed SAH as an essential renewable thermal-solar system more efficient and attractive so that this improvement pushes the industrial society toward more sustainable infrastructure.

***doi**: 10.5829/ijee.2021.12.02.09*

NOMENCLATURE

b	Height of air duct (m)	(u, v)	Velocity components (m/s)
c_p	Specific heat (kJ/kg K)	(x, y)	Horizontal and vertical coordinates (m)
D	Length of the horizontal duct (m)	**Greek symbols**	
F	Force per unit volume (N/m^3)	α	Thermal diffusivity (m^2/s)
g	Gravitational acceleration(m./s^2)	β	Volumetric thermal expansion (1/K)
h	Convection coefficient (W/m^2K)	ε	Turbulent kinetic energy (m^2/s^2)
k	thermal conductivity (W/m K)	δ	Chronicle delta
L	Length (m)	κ	Turbulence dissipation (m^2/s^3)
$\dot{m}$	Mass flow rate (kg/s)	μ_s	Lame's second parameter (Pa)
n	Normal direction	μ	Dynamic viscosity (Pa.s)
Pr	Prandtl number	ν	Poison ratio
p	Pressure (Pa)	ρ	Density (kg/m^3)
q''	Heat flux (W/m^2)	σ	Solid stress field (Pa)

*Corresponding Author Email: *ganj110@uk.ac.ir* (S. A. Gandjalikhan Nassab)

Please cite this article as: S. A. Gandjalikhan Nassab, M. Moein Addini, 2021. Performance Augmentation of Solar Air Heater for Space Heating Using a Flexible Flapping Guide Winglet, Iranian (Iranica) Journal of Energy and Environment, 12(2), pp.161-172. Doi: 10.5829/ijee.2021.12.02.09

Ra	Rayleigh number	Γ	Fluid stress field (Pa)
t	Time (s)	λ	Lame's first parameter (Pa)
T	Temperature (K)	**Subscript**	
$U_{s,i}$	VG displacement vector (m)	amb	Ambient
U_i	Flow velocity vector (m/s)	i, j	Indices

INTRODUCTION

The rapid growth of global demand for energy and fast depletion of fossil fuels all around the world together with their harmful effect on climate change and global warming is undeniable and hopefully have been recognized well by governments and researchers as a crucial problem. Consequently, it should be a part of researchers' mission to facilitate renewable energy as an essential pillar for sustainable development. The Sun radiation has the central role in using many renewable energies and avoiding from fossil fuel consumption.

The solar air heater is an inexpensive heat exchanger for converting solar radiative heat flux into air enthalpy, which may be used for space heating [1, 2]. As an essential renewable energy facility, SAHs also cover wide applications from drying agricultural products [1], cooking [3] and providing the required energy for air conditioning systems [4], etc. The last case is our concern in the present research work.

The solar air heaters are economically affordable, have simple configurations for installation, require less care for commissioning, and an absolutely free carrier fluid. These types of heat exchangers can effectively decrease the expense of energy consumption wherever they are involved [5]. However, SAHs usually operate with low thermal performance due to the low thermal conductivity of air, and also low convective coefficient between the air convection flow and the heated absorber surface [6]. There are several research works about technical solutions to increase the system performance [7–9]. The following ideas including the use of extruded surfaces such as baffles [10], straight and helicoidal spring shaped fins [11, 12], twisted-rib roughness [13], hyperbolic ribs [14], and employing V-shaped absorbers [15] were addressed by some investigations. The energy and exergy performances of an offset finned solar air heater were numerically investigated by Rai et al. [16]. In that study, parametric study was done to verify the effect of fins spacing and fins height at different mass flow rates on the performance of solar air heaters. It was concluded that that attaching offset finned below the absorber plate at low mass flow rates can lead to noticeable enhancement of exergy efficiency.

The variety of air heater configurations for improving the thermal efficiency was not limited to the above mentioned research works as the present author suggested the use of radiating working gas in planar SAH instead of air in a closed-loop system [17, 18]. It was revealed that the rate of energy conversion from solar irradiation into gas enthalpy increases because of the gas radiation effect.

All of the above-mentioned studies belong to the same group of heat transfer augmentation from the thermodynamic point of view. A new idea was introduced by the authors in their previous work, in which the vortex generation technique was introduced in air convection flow to change the dynamic of fluid movement by a winglet as turbulence promoter [19]. The flow vortices by a flapping elastic winglet attached to the absorber surface of SAH breaks down the thermal boundary layer by mixing process and leads to a higher rate of heat transfer from the heated surface. The main contribution of the present study, which focuses on the analysis of SAH for space heating (Figure 1), is using an elastic guide winglet at the corner of the heater duct for two purposes. The first is pushing the free convective airflow toward the absorber surface by a winglet as a guide tool and the second is generating flow vortices by the fluctuation of elastic winglet due to the fluid-solid interaction. There are several published papers about using VGs in forced convective flows. It was concluded that the vibration of elastic VG enhances the convection heat transfer by flow mixing and breaking the thermal boundary layer adjacent to the heated surfaces [20, 21].

Based on the recent literature review, using a flapping elastic guide winglet was not mentioned as a method of heat transfer enhancement in SAHs for space heating including the central vertical air duct with two elbows. The lack of literature on this subject motivates the author to study the VGs to improve the SAH thermal performance. As it will be seen later, the vortex generation technique by a flapping winglet that also has the role of a guide blade in the studied SAH causes a considerable improvement in the heater performance by increasing convective airflow rate and considerable reduction in absorber surface temperature. The former reduces the amount of heat transfer irreversibility in the convection heat transfer process by decreasing the temperature difference between the heated surface under constant heat flux and the convective airflow and also lowering the system's maximum temperature. For simulation, all of the governing equations are solved in transient two-way coupled fluid-structure interaction condition by the COMSOL multi-physics. Finally, the thermo-hydrodynamic characteristics of SAH with VG are presented and also comprehensive comparison is done with CSAH to show the pros and cons of vortex generation technique.

MODEL DESCRIPTION

In Figure 1, a schematic of the rectangular-shaped SAH, including the glass cover, air duct, absorber plate and elastic guide winglet is depicted. By natural convection, air enters from the inlet section and buoyancy force pushes it towards the outlet at the front. The thin absorber as a black body is exposed to constant heat flux transmitted from the glass cover, while the convection boundary condition for the glass cover exposed to ambient is considered with equivalent convection coefficient. The other main configuration of SAH , i.e., CSAH is also considered in this work. The lengths of SAH duct for its vertical and horizontal parts are equal to L and D and the air gap is denoted with b.

The thin rectangular shaped winglet made by very soft rubber is responsible for pushing the airflow toward the absorber and also for vortex generation. Table 1 provided its dimension and physical properties.

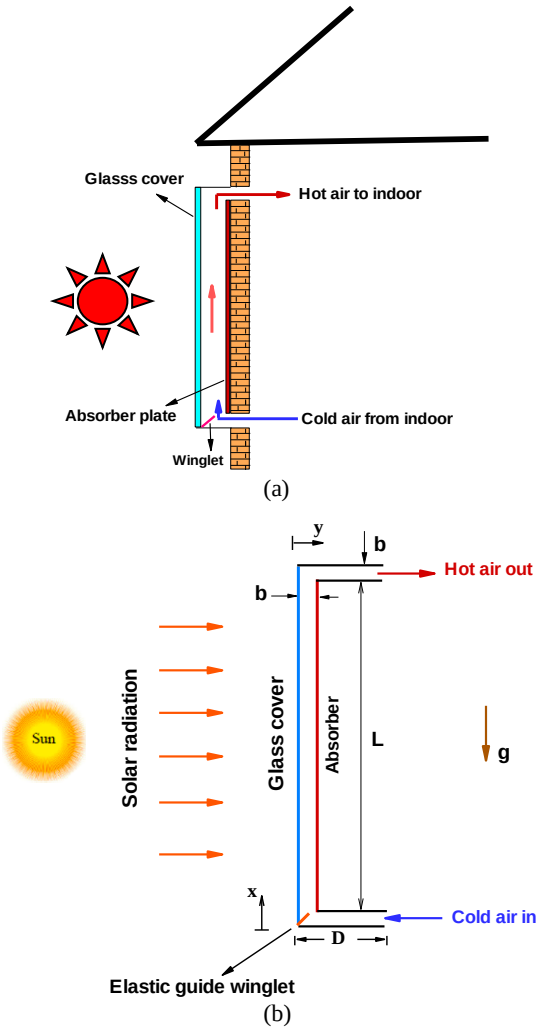

Figure 1. Geometry definition of SAH with elastic vortex generator; (a) Schematic of SAH for space heating, (b) Details of SAH geometry

Table 1. VG information and characteristic

Length	Thickness	Attacked angle	Module of elasticity	Poison ratio	Density
90 mm	3 mm	60°	0.15 MPa	0.4	1000 kg/m^3

THEORY

Inside the computational domain, because of the flapping winglet, the numerical simulation performed in transient form from the initial time when the stagnant air is at ambient temperature, up to semi-steady state while the system reaches to its periodic behavior. The fluid flow is determined by balancing the buoyancy head resulting from thermally induced density gradient and the friction head through the governing equations. Toward this end, the set of conservation equations including the mass, momentum and energy in their transient forms for free convection flow are solved numerically by progressing in time from t=0. In all test cases, the natural airflow is turbulent because the value of Rayleigh number defined as $Ra = g\rho\beta\, \boldsymbol{q}'' b^4/k\mu\alpha$ which is in the order of 10^8 [22]. The numerical findings are compared with both theoretical and experimental data reported in the relevant literature.

Governing equation

The set of governing equations for transient Newtonian incompressible turbulent airflow consist of conservation of mass, momentum and energy which are coupled with the vibration of VG through Fluid-Solid Interaction (FSI) is presented in Equations (1) to (4).

$$\nabla . V = 0 \tag{1}$$

$$\frac{\partial(\rho V)}{\partial t} + V.\nabla(\rho V) = -\nabla P + \nabla.[(\mu + \mu_t)(\nabla V + \nabla V^T)] + (\rho - \rho_o)g - \nabla\left(\frac{2}{3}\mu\nabla.V\right) + F_{ext.VG} \tag{2}$$

$$\frac{\partial(\rho C_p T)}{\partial t} + V.\nabla(\rho C_p T) = \nabla.\left[\left(k_{th} + \frac{\mu_t}{Pr_t}\right)\nabla T\right] \tag{3}$$

$$\frac{\partial(\rho\kappa)}{\partial t} + V.\nabla(\rho\kappa) = \nabla.\left(\left(\mu + \frac{\mu_t}{\sigma_k}\right)\nabla k\right) + P_k + P_b - \rho\epsilon + S_k \tag{4}$$

$$\frac{\partial(\rho\varepsilon)}{\partial t} + V.\nabla(\rho\varepsilon) = \nabla.\left(\left(\mu + \frac{\mu_t}{\sigma_\epsilon}\right)\nabla\epsilon\right) + C_1\frac{\epsilon}{k}(P_k + C_3P_b) - C_2\rho\frac{\epsilon^2}{k} + S_\epsilon \tag{5}$$

where, $\mu_t = C_\mu \frac{\rho k^2}{\epsilon}$ is the turbulent viscosity, P_k, P_b denotes turbulent production and buoyancy production, and C_1, C_2, C_3 are constant. Some informations are tabulated in Table 2 and more details can be found in literature [23]. All thermo-physical properties of air assumed to be constant, except the density where, the

Table 2. Summary of methodology

Flow regime	Flow modeling method	Algorithm of solution	Rayleigh No.	Reynolds No.
Turbulent	Standard $k-\varepsilon$	SIMPLE	10^8	3000
C_1	C_2	C_3	σ_ϵ	σ_k
1.44	1.92	0.09	1.3	1.0

Boussinesq approximation was used for temperature dependent density estimation. The well-known standard $k-\varepsilon$ method [23] is used for computation of turbulent stress and heat flux with the RANS problem.

In momentum equations, $F_{ext.VG}$ is the external force on the fluid due to transient vibration of elastic vortex generator. This situation is interdisciplinary subject which is so-called two-way modeling in computational fluid dynamic [24].

The equation of motion for computing the oscillation of 2-D flapping VG exposed to the convection flow can be driven as [22]:

$$(\lambda+\mu_s)\frac{\partial}{\partial x_i}\left(\frac{\partial U_{sj}}{\partial x_i}\right)+\mu_s\frac{\partial}{\partial x_j}\left(\frac{\partial U_{si}}{\partial x_j}\right)=\rho_s\ddot{U_{s\,i}} \quad (6)$$

where, U_{si} is the displacement vector of the elastic sheet. More details about the equations govern to the displacement of elastic winglet were given in the article by Li et al. [21].

Boundary condition

The following initial and boundary conditions were imposed in numerical solution of the governing equations:

- At t=0, the air is stagnant with ambient temperature (293 K).
- At the inlet and outlet sections, the air is at ambient pressure.
- No slip condition is considered in velocity computation.
- The air temperature at the outlet was corrected via the energy balance during the iterative procedure.
- On the absorber surface which is assumed black body, a constant heat flux was assigned (q'' =800 W/m^2), while on the boundary surface of glass cover exposed to surrounding, the third kind of boundary condition with equivalent convection coefficient of $h=5\ W/(m^2\mathrm{K})$ and $T_{amb}=293\ K$ was employed.
- The continuous boundary conditions of the velocity and stress fields of VG yield to the following criteria.

$$U_i=\dot{U}_{si} \quad (7)$$

$$\sigma_{ij}n_j=\Gamma_{ij}n_j \quad (8)$$

where, n_j is the local normal pointing outward from the surface. The stress fields inside the solid and fluid phases can be computed by [21]:

$$\sigma_{ij}=\mu_s\left[U_{si,j}+U_{sj,i}\right]+\frac{\lambda}{2}tr\left(U_{si,j}+U_{sj,i}\right) \quad (9)$$

$$\Gamma_{ij}=-p\delta_{ij}+\mu\left[U_{i,j}+U_{j,i}\right]-\frac{2}{3}\mu U_{i,i}\delta_{ij} \quad (10)$$

Due to VG vibration, the computational domain including flow field was considered as the deforming region and the continuity, momentum and energy equations were solved with moving mesh technique. The finite element method (FEM) was used in numerical solution of the governing equations, while, the unstructured triangular grid generation method was employed for discretization of the computational domain including the flapping guide winglet and the convective airflow as shown in Figure 2. At each time step, all of the governing equations were solved simultaneously for obtaining the converged solutions for pressure, velocity and temperature of air flow and also the VG displacement. These computations started from t=0, while the air and VG are at stagnant position, and all of the SAH's components are at ambient temperature. This procedure continued with time marching until a time periodic behavior was observed. This condition is called semi steady state in the paper.

Mesh

Grid dependency was verified by using different grid sizes in the computational domain. Based on Table 3 in which the airflow rate is tabulated at different mesh sizes through the mesh independency check, the grid configuration #3 was selected at which the flow rate value does not change much respect to the grid configuration #4 that has finer mesh and lower grid size. The unstructured triangular grid generation method was used for the 2D geometry of SAH, Figure 2, such that near the walls mesh was refined to precisely capture the high gradient of dependent variables, especially around vibrating EVG. As it is summarized in Table 3, the number of nodes in the selected unstructured optimum grid is 9648 with the average element's quality of 0.91.

As the set of governing equations was solved iteratively at each time step, convergence criteria were needed to distinguish the converged solution. The minimum residuals for mass, momentum and energy are tabulated in Table 4. The numerical solution starts at t=0 while the stagnant air is at ambient temperature. Besides, the maximum time step of 0.006 s was employed in time marching up to semi-steady condition while the system reaches to its periodic behavior with time.

The deformable elastic winglet inside convective airflow not only experiences large deformations due to the receiving momentum from moving fluid, but also its transient oscillations interact with surrounding continuous media, such that its reaction also exerts a surface force on fluid as well. This situation is called two-way modeling which causes many complexities. The complete FSI formulation that leads to form $F_{ext.VG}$ is

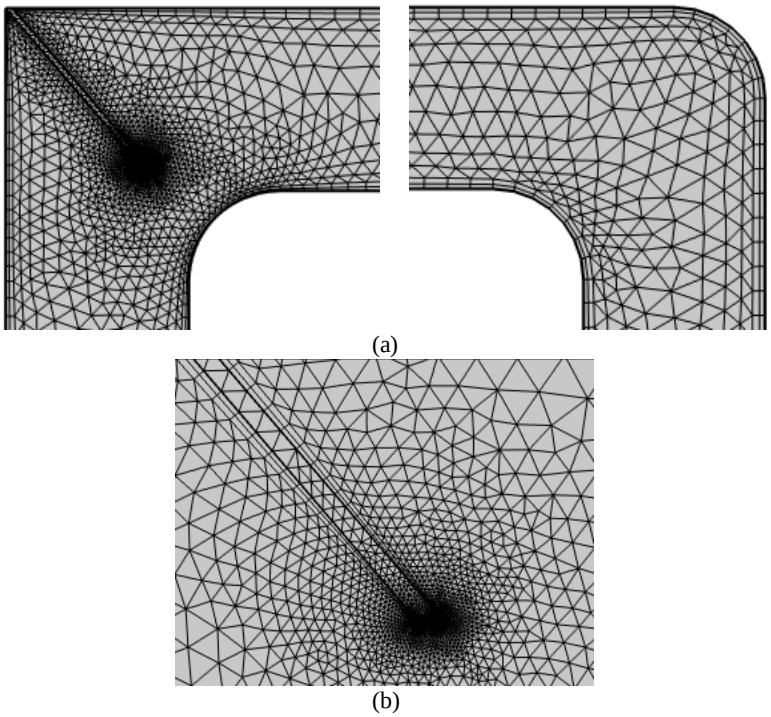

Figure 2. The unstructured triangular mesh. (a) High enlarged discretized domain in the elbows, (b) Grids near to VG

Table 3. Mesh dependency check

Tracked parameter	Mesh #1 4554 element		Mesh #2 6905 element		Mesh #3 9648 element		Mesh #4 12233 element	
	value	% of variation	value	% of variation	value	% of variation	value	% of variation
Flow rate [m^2/s]	0.0482	-	0.0611	27	0.0631	3	0.0635	0.6
Computational time (min)	19		27		35		49	

provided by COMSOL Multiphysics, and this software was used in the present numerical simulation. It should be mentioned that all the computations were carried out using a computer with Intel(R) Core (TM) i5-3210M cpu@2.50 GHz. In Table 3, the computational time for all of the mesh sizes including the optimum grid is also reported.

VALIDATION

The numerical results of present simulation were validated first with the theoretical findings reported in the literature [21]. In that work, a forced convective turbulent airflow in a channel with an elastic VG attached to the lower wall was numerically simulated. Both heated walls are in the same constant high temperature. In this test case, the same mesh and configuration, was adapted to the dimenssions of geometry exactly as it was considered in the literature [21]. The averaged Nusselt number on the lower heated wall is calculated at different values of Reynolds number and different modulus of elasticity (See Figure 3). As it was expected, an increasing trend for Nusselt number is seen with increasing in Reynolds number. Also, it is seen that the averaged Nusselt number is directly proportional to the VG 's modul of elasticity in the region $0.4 \leq E \leq 1$ MPa after which a reverse behavior is observed. So, an optimum value exists for having the maximum convection coefficient. However, good agreement is seen between the present numerical results based on the FEM simulation and the findings by Li et al. [21].

Table 4. Minimum considered residual for governing equations as convergence criteria

Conservation of mass	Conservation of momentum	Conservation of energy
5×10^{-4}	5×10^{-4}	10^{-4}

A long vertical channel with a heated wall in which the natural convection airflows because of the buoyancy effect was simulated in the second test case for validation.

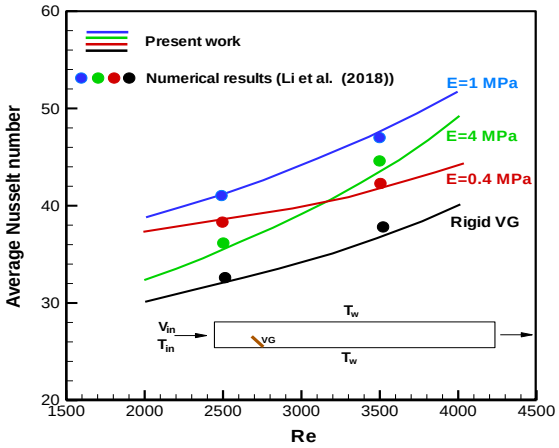

Figure 3. Average Nusselt number on the lower wall vs Reynolds number at different values of winglet modulus of elasticity [21]

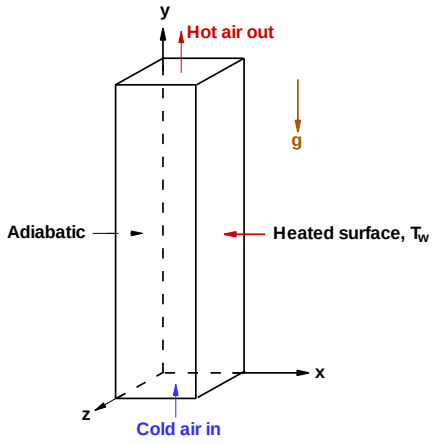

(a)

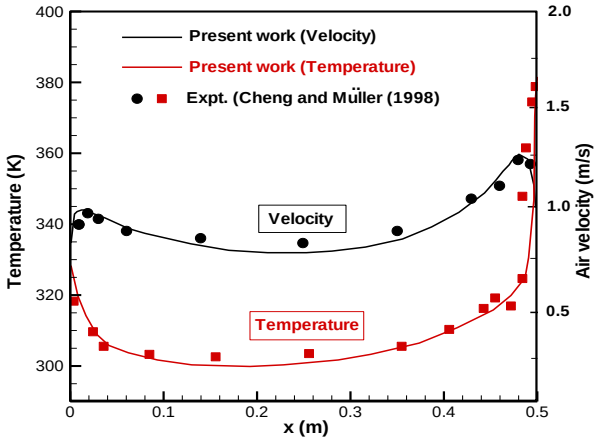

(b)

Figure 4. Schematic of the simulated chimney, (a), Temperature and velocity distributions across the channel at y=7.8 m (b), and comparison with experiment [25]

This thermal system was also experimentally investigated by Cheng and Müller [25]. It has a rectangular-shaped channel whose height is 8 m and the width and depth is 0.5 m. Due to the adiabatic top and bottom surfaces in three dimensional geometry, a two dimensional model was assigned at the mid-plane ($z = L_z/2$), which is dimensionally identical to the experimental set-up. One wall of the channel is adiabatic and the other is kept at constant temperature 423 K. For this test case, the value of Rayleigh number is equal to 5×10^{12} correspondence to the turbulent natural convective flow. The computed velocity and temperature variations across the channel width at y=7.8 m have been compared with experiment in Figure 4. Because of the good consistencies, it can be concluded that the present numerical simulation can predict both flow and thermal characteristic of SAHs with natural turbulent air convection flow.

RESULTS AND DISCUSSION

After the validation of present numerical simulation, from grid generation to model adoption and convergency, results of numerical findings are presented in this section. In the beginning, the configuration of SAH with vortex generator is illustrated in detail and the physics behind the advantage of VG exploitation is explained and then a comparison will be made with CSAH at the end of this section.

SAH with VG

In the configuration of solar chimney with elastic vortex generator, the most important features that make all advantages are the role of winglet as a guide blade that pushes the natural airflow against the absorber surface and the natural oscillation of the VG because of the FSI. In Figure 5, the evolution of air velocity along the chimney at different times shows how the flow field evolves. As seen, computations are performed during the time interval $0 \leq t \leq 15$ s after which the system approaches to a time period behavior, but still the natural airflow remains unsteady. Figure 5 depicts that the airflow initiates closed to the heater absorber because of the buoyancy effect at early times and then it develops in the whole region of the chimney duct from the inlet section toward the outlet due to continuity requirement. After t=3 s, the vibration of flapping winglet introduces some flow vortices into the convective flow and this phenomenon enhances by progressing in time with higher frequency and larger deformation of VG. In most of the captured moments, the high local values of air velocity occur very close to the hot absorber surface. The generated flow vortices and the wavy form of convective flow are known to be responsible for heat transfer enhancement that leads to more penetration of thermal energy from heated surface into the free convective airflow (Figure 6). As it will be studied with more details, this behavior causes to higher volumetric airflow rate and considerable decrease in the absorber temperature.

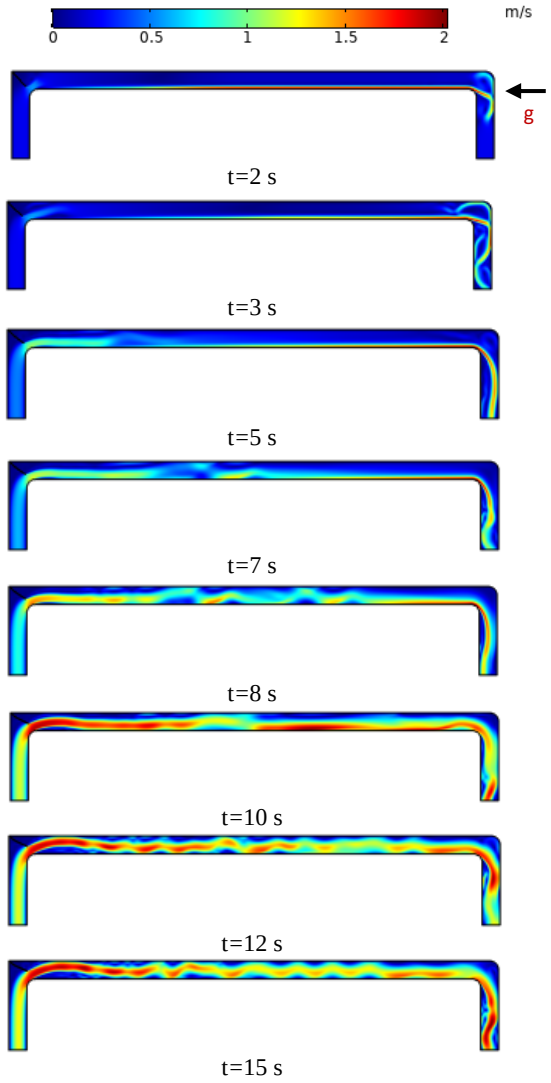

Figure 5. Velocity magnitude contours at different times

The temperature contours at different times are potted in Figure 7. The mixing effect of winglet that leads to breaking the thermal boundary layer and enhancing the convection heat transfer is clearly observed. The air temperature in the zoomed area near to the flapping VG is also presented in Figure 8 in which the deformation of elastic winglet at different times can also be seen.

To study more about the effect of VG on thermal behavior of SAH, the air temperature distributions along the centerline of vertical duct of heater are plotted in Figure 9 at four different times. As seen, the air temperature increases with time such that the vibration of VG and flow vortices causes temperature fluctuation along the flow direction. This is the main purpose of using

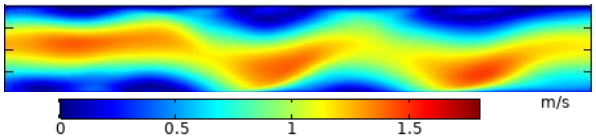

Figure 6. Enlarged velocity magnitude contours inside the vertical duct section in $0.8 \leq x \leq 1.35\ m$ at t=15 s

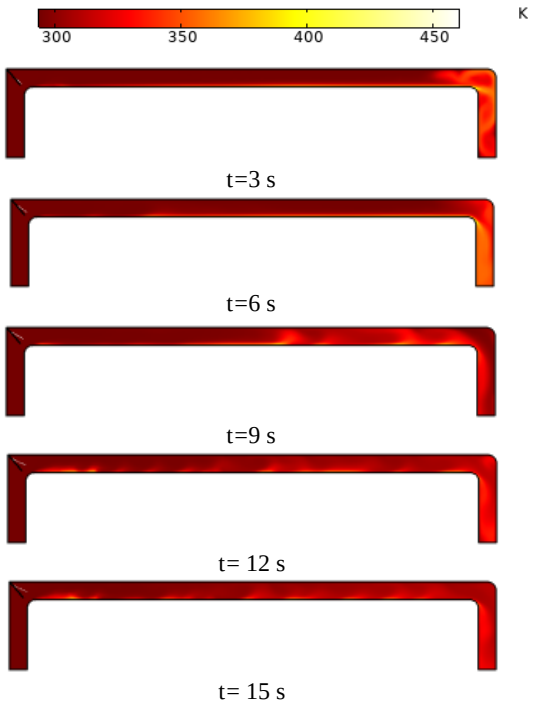

Figure 7. Temperature contours at different times

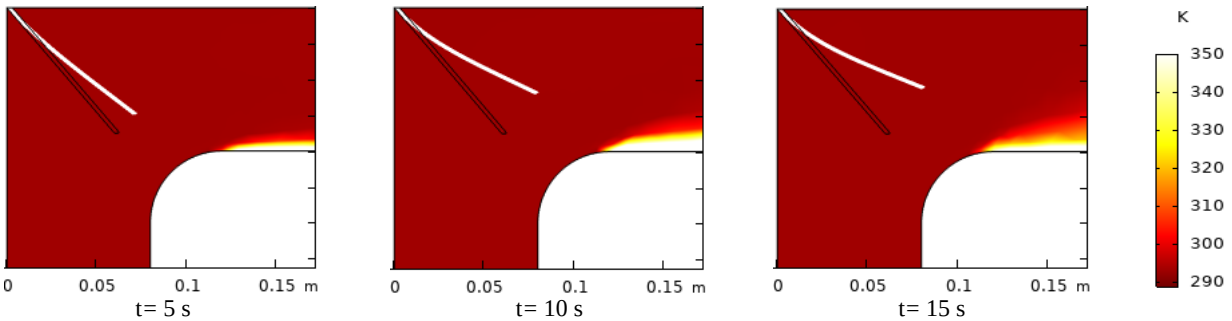

Figure 8. Enlarged temperature contours near to VG

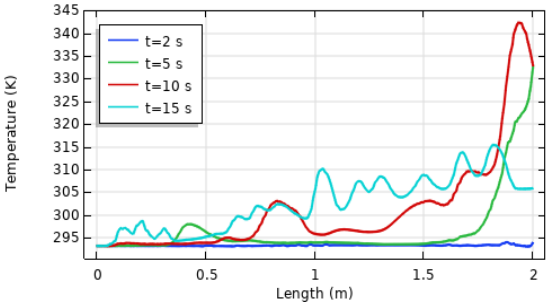

Figure 9. The air temperature distribution along the centerline of the vertical duct of SAH

flapping winglet that enhances the convection heat transfer in natural airflow. This effect also resulted in a fluctuating pattern for the absorber surface temperature as demonstrated in Figure 10. As shown, by progressing in time and introducing flow vortices into the free convection flow by flapping winglet, the absorber temperature decreases considerably and gets high fluctuating pattern. It should be noted that the maximu m temperature inside SAH takes place on the absorber surface and decrease in this temperature resulted in more reversible convective heat transfer.

To show the vibration of elastic winglet, for point A on the tip of VG, the x component of displacement due to FSI is drawn in Figure 11. This figure shows large deformation of winglet and its increasing trend with time, until the vibration reaches to a periodic situation after t=15 s. This is the main aim of using VG that introduces flow vortices with mixing effect in convective airflow.

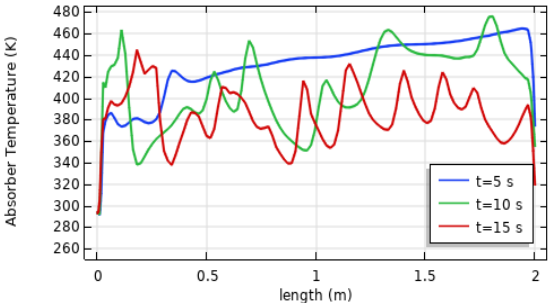

Figure 10. Absorber temperature variation along its length

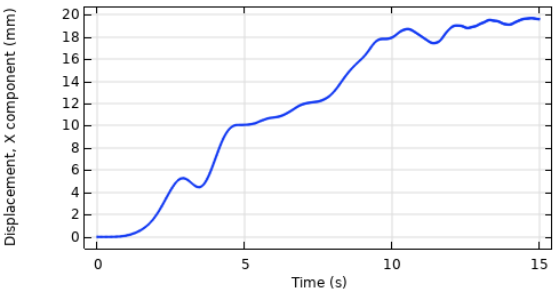

Figure 11. The x-displacement component of the tip of VG with time

Finally, the air pressure contours at different times are shown in Figure 12. As seen, the buoyant airflow behaves as an isobar one with less than 2 Pa in pressure variation. It is the nature of free convective flows in which the density gradient is the only driving force.

SAH without VG (CSAH)

For illustrating the positive effect of elastic guide VG in improving the SAH performance, the velocity and temperature contours of airflow in CSAH are shown in Figures 13 and 14 for comparison. Velocity magnitude

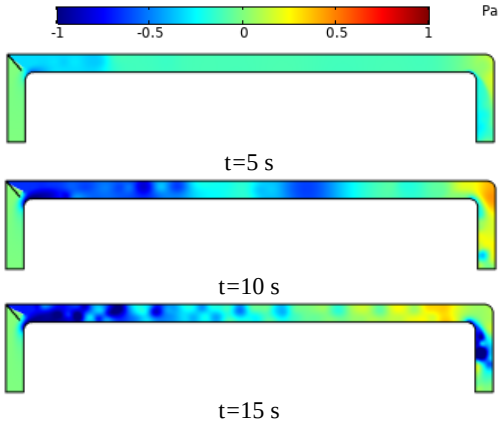

Figure 12. Pressure contours at different times

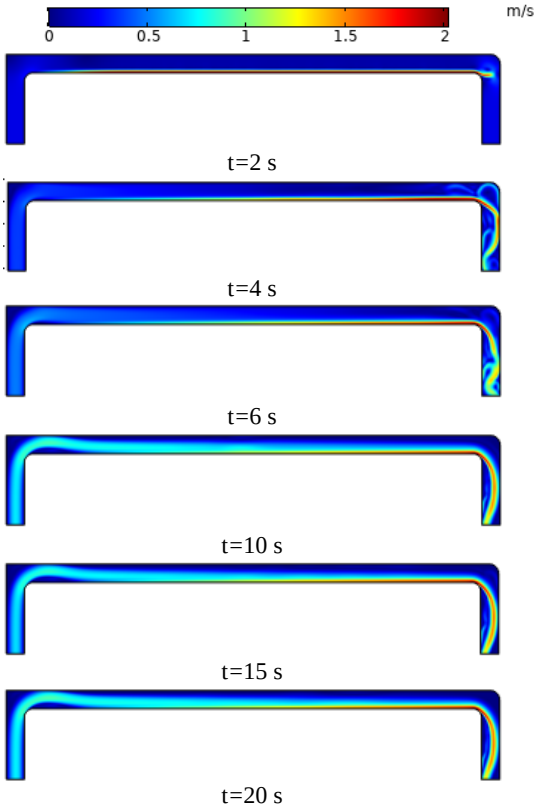

Figure 13. Time history of the velocity magnitude contours

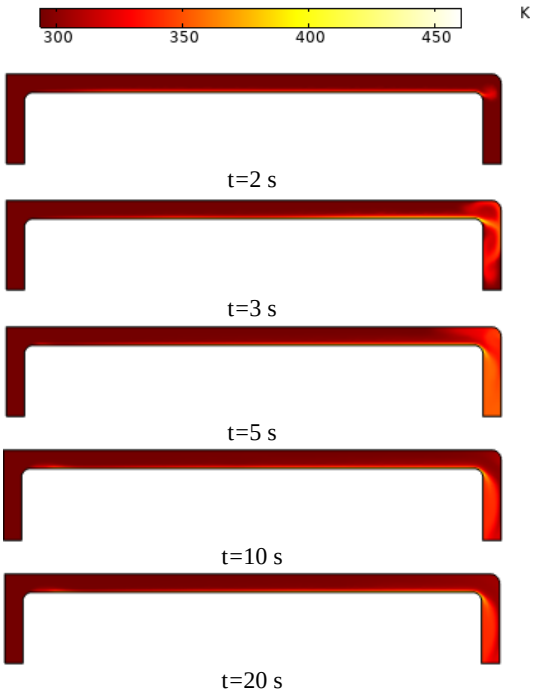

Figure 14. Time history of isotherms

contours demonstrate that airflow locally accelerates and increases its velocity to satisfy the continuity equation. It is seen that only a thin layer of working gas adjacent to the heated surface is effectively affected by the absorber surface, especially this trend is observed in temperature contours. Although, the heat penetration due to conduction expands this thin layer by progressing in time, but it does not reach to the air layer adjacent to the glass cover. It is evident that this characteristic leads to low thermal performance for SAH.

The pressure contours plot is presented in Figure 15 at t=20s, after which the system approaches to its periodic behavior. This figure shows again an almost isobar flow in CSAH as it was observed before for SAH with VG. As seen, Figure 15 depicts low pressure domains in the recirculated regions downstream the two elbows.

The temperature distributions along the absorber surface at different times are drawn in Figure 16. Except, on the absorber surface downstream of the first elbow which has a local maximum temperature after the separation point and then a local minimum temperature at

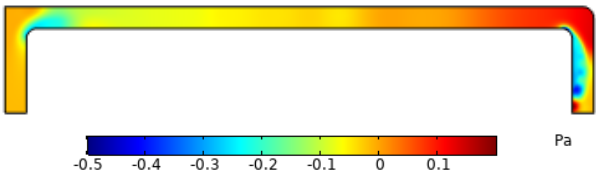

Figure 15. Pressure contours at t=20 s

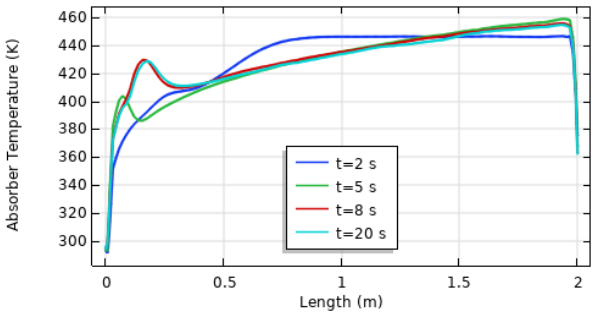

Figure 16. Distributions of absorber surface temperature at different times

the reattachment point, the temperature distribution does not have any fluctuation which was observed before for SAHs with elastic VG. This is due to this fact that there are not any flow vortices and mixing process in the natural airflow through CSAHs. If one compares this figure with Figure 10, it can be found that the absorber of CSAH is at higher temperature, and this behavior can show the positive effect of vortex generation technique in convection enhancement.

Comparison between two configurations

Two main parameters in SAHs which show the performance of heaters are airflow rate and bulk temperature at the outlet section. The time histories of these two parameters for SAH with VG and CSAH are plotted in Figures 17 and 18.

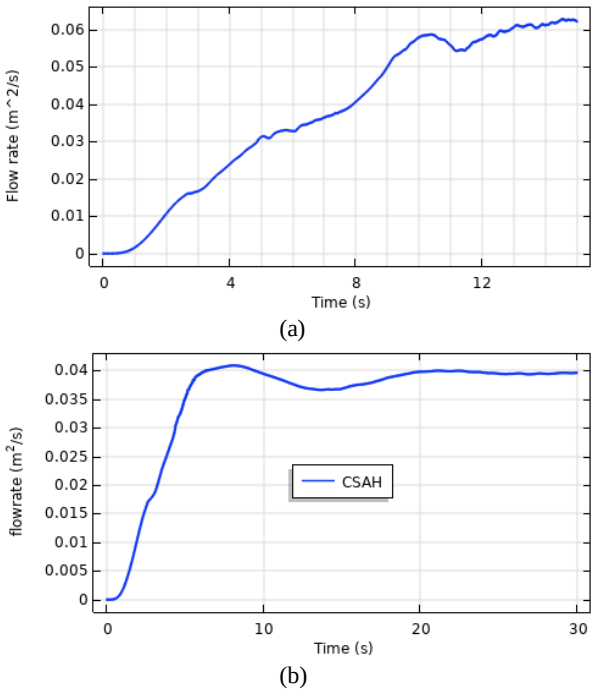

Figure 17. Time histories of volumetric airflow rate; (a) SAH with VG, (b) CSAH

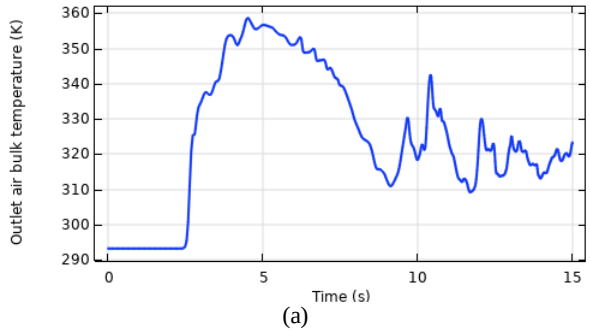

(a)

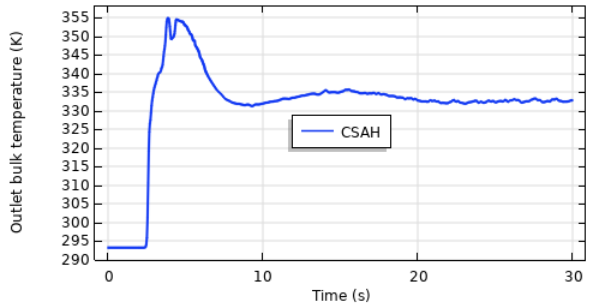

(b)

Figure 18. Variation of air outlet bulk temperature vs time; (a) SAH with VG, (b) CSAH

As the absorber plate of SAH is exposed to the sun heat flux, buoyant force drives the quiescence air into motion such that the variation of airflow rate for these two configurations has almost the same trend: increased from zero and reaches its maximum value after which the system gets its periodic behavior. At this time (t=15 s), while the heater passes its transient time period, the averaged values of flow rate for these configurations are computed and tabulated in Table 5.

Based on this table, about 58% increase in air flow rate is seen due to the vortex generation and mixing effect of VG. This is a great improvement in the performance of SAH , because the absorber temperature is much affected by the airflow rate, such that higher air velocity resulted in higher convection coefficient and caused the absorber's temperature to come down.

From the beginning of the numerical experiment, the incoming radiative flux warms up the absorber surface and causes a higher temperature difference between the absorber and its adjacent working gas. This leads to a higher body force to drive the neighboring balk of fluid faster and faster. As the airflow rate grows gradually, the heat transfer rate will increase and consequently cause the absorber's temperature to come down. It means that the outlet temperature must have a maximum value somewhere close to the starting time. This maximum value for these two configurations takes place about t=5 s. The maximum recorded outlet temperature belongs to CSAH. Moreover, the air bulk temperature along the CSAH has no a considerable temperature fluctuation as there is no reason to disturb the airflow. But the air temperature in SAH with VG shows fluctuation over time.

Table 5. The time averaged value of flow rate

Configurations	SAH with VG	CSAH
Time average value of flow rate [l/s]	63	40
Percentage of enhancement respect to CSAH	58%	-

To compare SAH thermal performance for these two configurations, the outlet bulk temperature difference is defined as $\Delta\bar{T} = \bar{T}_{out} - T_{in}$, where T_{in} is the inlet temperature equal to 293 K. The $\bar{T}_{out}$ is the time-averaged value of outlet temperature while SAH reaches to its period behavior. By computing the value of $\Delta\bar{T}$ for a conventional CSAH (40 K) and comparing it with its corresponding value for SAH with VG (25 K), 37% decrease in temperature difference can be computed due to vortex generation. It should be noted again that because of the constant heat flux condition on the absorber surface for the studied two configurations and due to very small value of heat transfer from the glass cover into the surrounding, the total rate of convection heat transfer i.e. $\dot{m}c_p\Delta\bar{T}$ remains almost constant , but it is worth mentioning that using the elastic guide winglet leads to a huge temeperature decrease on absorber plate, i.e. from 421 K in CSAH to 382 K with vortex generation technique (Figures 10 and 16).

CONCLUSION

The present numerical simulation is dedicated to the sustainable solution for the exploitation of renewable energy facility through heat transfer augmentation of natural airflow in SAHs for space heating by proposing a new concept of employing an elastic guide winglet as a passive vortex generator at the corner of solar chimney. In addition to the role of winglet as a guide blade to push the free convective airflow against the heated surface, the passive method of vortex generation by flapping VG induces a new active dynamic into the airflow. In numerical simulation, the set of governing equations including the conservations of mass, momentum and energy for the turbulent free convection coupled with fluid-solid interaction with employing the well-known $k-\varepsilon$ turbulent model was solved in transient condition by the FEM. Numerical results reveal significant improvement for the proposed novel SAH equipped with elastic winglet, as it offers a higher flow rate (56%) and lower absorber temperature (9%), respect to CSAH. The outstanding performance of the proposed idea could be implemented in design of SAH for space heating to make it more efficient and attractive.

DECLARATION OF COMPETING INTEREST

The author declares that there was no known competing financial interests or personal relationships that could have appeared to influence the work reported in this paper.

FUNDING

This research was not funded by any organization and no financial support was allocated.

REFERENCES

1. Gill, R. S., Singh, S., and Singh, P. P. 2012. "Low cost solar air heater." *Energy Conversion and Management*, 57, pp.131–142. https://doi.org/10.1016/j.enconman.2011.12.019
2. Tuncer, A. D., Khanlari, A., Sözen, A., Gürbüz, E. Y., Şirin, C., and Gungor, A. 2020. "Energy-exergy and enviro-economic survey of solar air heaters with various air channel modifications." *Renewable Energy*, 160, pp.67–85. https://doi.org/10.1016/j.renene.2020.06.087
3. Aramesh, M., Ghalebani, M., Kasaeian, A., Zamani, H., Lorenzini, G., Mahian, O., and Wongwises, S. 2019. "A review of recent advances in solar cooking technology." *Renewable Energy*, 140, pp.419–435. https://doi.org/10.1016/j.renene.2019.03.021
4. Kalogirou, S. A. 2004. "Solar thermal collectors and applications." *Progress in Energy and Combustion Science*, 30(3), pp.231–295. https://doi.org/10.1016/j.pecs.2004.02.001
5. Kabeel, A. E., Hamed, M. H., Omara, Z. M., and Kandeal, A. W. 2017. "Solar air heaters: Design configurations, improvement methods and applications – A detailed review." *Renewable and Sustainable Energy Reviews*, 70(November 2015), pp.1189–1206. https://doi.org/10.1016/j.rser.2016.12.021
6. Singh, A. P., and Singh, O. P. 2019. "Thermo-hydraulic performance enhancement of convex-concave natural convection solar air heaters." *Solar Energy*, 183(October 2018), pp.146–161. https://doi.org/10.1016/j.solener.2019.03.006
7. Singh, S. 2020. "Experimental and numerical investigations of a single and double pass porous serpentine wavy wiremesh packed bed solar air heater." *Renewable Energy*, 145, pp.1361–1387. https://doi.org/10.1016/j.renene.2019.06.137
8. Fan, W., Kokogiannakis, G., and Ma, Z. 2019. "Optimisation of life cycle performance of a double-pass photovoltaic thermal-solar air heater with heat pipes." *Renewable Energy*, 138, pp.90–105. https://doi.org/10.1016/j.renene.2019.01.078
9. Singh, A. P., and Singh, O. P. 2020. "Curved vs. flat solar air heater: Performance evaluation under diverse environmental conditions." *Renewable Energy*, 145, pp.2056–2073. https://doi.org/10.1016/j.renene.2019.07.090
10. Bensaci, C.-E., Moummi, A., Sanchez de la Flor, F. J., Rodriguez Jara, E. A., Rincon-Casado, A., and Ruiz-Pardo, A. 2020. "Numerical and experimental study of the heat transfer and hydraulic performance of solar air heaters with different baffle positions." *Renewable Energy*, 155, pp.1231–1244. https://doi.org/10.1016/j.renene.2020.04.017
11. Priyam, A., and Chand, P. 2018. "Effect of wavelength and amplitude on the performance of wavy finned absorber solar air heater." *Renewable Energy*, 119, pp.690–702. https://doi.org/10.1016/j.renene.2017.12.010
12. Arunkumar, H. S., Kumar, S., and Karanth, K. V. 2020. "Analysis of a solar air heater for augmented thermohydraulic performance using helicoidal spring shaped fins-A numerical study." *Renewable Energy*, 160, pp.297–311. https://doi.org/10.1016/j.renene.2020.06.098
13. Kumar, A., and Layek, A. 2019. "Nusselt number and friction factor correlation of solar air heater having twisted-rib roughness on absorber plate." *Renewable Energy*, 130, pp.687–699. https://doi.org/10.1016/j.renene.2018.06.076
14. Thakur, D. S., Khan, M. K., and Pathak, M. 2017. "Performance evaluation of solar air heater with novel hyperbolic rib geometry." *Renewable Energy*, 105, pp.786–797. https://doi.org/10.1016/j.renene.2016.12.092
15. Jin, D., Quan, S., Zuo, J., and Xu, S. 2019. "Numerical investigation of heat transfer enhancement in a solar air heater roughened by multiple V-shaped ribs." *Renewable Energy*, 134, pp.78–88. https://doi.org/10.1016/j.renene.2018.11.016
16. Rai, S., Chand, P., and Sharma, S. P. 2016. "Investigation of an Offset Finned Solar Air Heater Based on Energy and Exergy Performance." *Iranian (Iranica) Journal of Energy and Environment*, 7(3), pp.212–220. https://doi.org/10.5829/idosi.ijee.2016.07.03.01
17. Rayeni, A. D., and Nassab, S. A. G. 2020. "Effects of Gas Radiation on Thermal Performances of Single and Double Flow Plane Solar Heaters." *International Journal of Engineering, Transaction C: Aspects*, 33(6), pp.1156–1166. https://doi.org/10.5829/ije.2020.33.06c.14
18. Foruzan Nia, M., Gandjalikhan Nassab, S. A., and Ansari, A. B. 2020. "Numerical Simulation of Flow and Thermal Behavior of Radiating Gas Flow in Plane Solar Heaters." *Journal of Thermal Science and Engineering Applications*, 12(3), pp.1–8. https://doi.org/10.1115/1.4044756
19. Sheikhnejad, Y., and Gandjalikhan Nassab, S. A. 2021. "Enhancement of solar chimney performance by passive vortex generator." *Renewable Energy*, 169, pp.437–450. https://doi.org/10.1016/j.renene.2021.01.026
20. Ali, S., Menanteau, S., Habchi, C., Lemenand, T., and Harion, J.-L. 2016. "Heat transfer and mixing enhancement by using multiple freely oscillating flexible vortex generators." *Applied Thermal Engineering*, 105, pp.276–289. https://doi.org/10.1016/j.applthermaleng.2016.04.130
21. Li, Z., Xu, X., Li, K., Chen, Y., Huang, G., Chen, C., and Chen, C.-H. 2018. "A flapping vortex generator for heat transfer enhancement in a rectangular airside fin." *International Journal of Heat and Mass Transfer*, 118, pp.1340–1356. https://doi.org/10.1016/j.ijheatmasstransfer.2017.11.067
22. La Pica, A., Rodonò, G., and Volpes, R. 1993. "An experimental investigation on natural convection of air in a vertical channel." *International Journal of Heat and Mass Transfer*, 36(3), pp.611–616. https://doi.org/10.1016/0017-9310(93)80036-T
23. Singh, A. P., Akshayveer, Kumar, A., and Singh, O. P. 2019. "Designs for high flow natural convection solar air heaters." *Solar Energy*, 193(August), pp.724–737. https://doi.org/10.1016/j.solener.2019.10.010
24. Le Tallec, P., and Mouro, J. 2001. "Fluid structure interaction with large structural displacements." *Computer Methods in Applied Mechanics and Engineering*, 190(24–25), pp.3039–3067. https://doi.org/10.1016/S0045-7825(00)00381-9
25. Cheng, X., and Müller, U. 1998. "Turbulent natural convection coupled with thermal radiation in large vertical channels with asymmetric heating." *International Journal of Heat and Mass Transfer*, 41(12), pp.1681–1692. https://doi.org/10.1016/S0017-9310(97)00303-7

Persian Abstract

چکیده

در این مقاله طرح جدیدی از یک هواگرمکن خورشیدی به منظور گرمایش ساختمان ارائه گردیده که در آن از یک بالک منعطف استفاده شده است. علاوه بر نقش هدایت جریان سیال توسط پره راهنما، در اثرجود نیروهای سازه-سیال بالک حالت ارتعاشی داشته و نقش مولد گردابه را نیز بازی می‌کند. .وجود گردابه در جریان واختلاط ناشی از آن، شکست لایه مرزی حرارتی را باعث شده و نهایتاً افزایش شدت انتقال حرارت جابجایی را به دنبال دارد. در شبیه‌سازی مسئله باروش المان محدود، معادلات حاکم در شرایط گذرا شامل پیوستگی، ممنتم و انرژی با در نظر داشتن نیروهای بین سازه و سیال به صورت دو طرفه، توسط نرم افزار کامسول حل عددی شده و از مدل $k-\varepsilon$ در مدلسازی جریان آشفته استفاده گردیده است. مسائل متعددی در این کار حل شده و مقایسه‌ای هم بین نتایج با وجود پره راهنما و بدون وجود آن صورت پذیرفته است. نتایج نشان‌دهنده کارآیی مثبت بالک در عملکرد هواگرمکن خورشیدی بوده و معادل ۵۶٪ افزایش در دبی جریان طبیعی هوا و ۹٪ کاهش در دمای متوسط صفحه جاذب بواسطه ارتعاش مولد گردابه دیده می‌شود. اما دمای هوای خروجی با کاهش ۱۴ در صدی مواجه بوده که دلیل آن، کارکرد هواگرمکن در دبی حجمی بالا بواسطه وجود بالک می‌باشد. این ایده می‌تواند در جهت افزایش کارآیی سیستم‌های خورشیدی در مصارف مختلف صنعتی بکار آید.